https://doi.org/10.5194/egusphere-2025-3956
Preprint. Discussion started: 12 September 2025
© Author(s) 2025. CC BY 4.0 License.

Response relationship between atmospheric O_3 and its precursors in Beijing based on smog chamber simulation and a revised MCM model

Jialin Lu[1, 2], Tianzeng Chen[1, 2 *], Jun Liu[1, 2], Huiying Xuan[1, 2], Peng Zhang[1, 2], Qingxin Ma[2, 3], Yonghong Wang[1, 2], Hao Li[1, 2], Biwu Chu[2, 3, *], Hong He[1, 2, 4]

[1]Laboratory of Atmospheric Environment and Pollution Control, Research Center for Eco-Environmental Sciences, Chinese Academy of Sciences, Beijing 100085, China

[2]University of Chinese Academy of Sciences, Beijing 100049, China

[3]State Key Laboratory of Regional Environment and Sustainability, Research Center for Eco-Environmental Sciences, Chinese Academy of Sciences, Beijing, 100085, China

[4]State Key Laboratory of Advanced Environmental Technology, Institute of Urban Environment, Xiamen 361021, China

Correspondence to: tzchen@rcees.ac.cn (Tianzeng Chen) and bwchu@rcees.ac.cn (Biwu Chu)

Abstract. Ozone (O_3) pollution has been receiving increasing attention, but its simulation performance in models remains unsatisfactory. This study characterized the response relationship between O_3 and its precursors in the atmospheric relavant condition through a combination of smog chamber experiments and Master Chemical Mechanism (MCM) box model. By adding chamber wall related reaction mechanisms, the model achieved significant improvement in simulating O_3 with an Normalized Mean Bias (NMB) value changing from -76.1 % to -12.7 %. The enhanced model was subsequently extended to the ambient atmospheric conditions in the Daxing District of Beijing, incorporating the parameterization of ground related reactions, heterogeneous reactions of Nitrogen Dioxide (NO_2), and unidentified NO_2 sinks. Compared to basic model, the resulting revised model demonstrated substantially enhanced accuracy in simulating ambient O_3 concentrations with an Normalized Mean Bias (NMB) value changing from 113.8 % to -5.2 % and enhanced O_3 formation sensitivity to Volatile Organic Compounds (VOCs) in Daxing District. These findings underscore that incorporating interface mediated chemical processes and accounting for unidentified NO_2 sinks into model is critical for determining the sensitivity of O_3 formation and optimizing regional O_3 pollution control strategies.

1 Introduction

Ozone (O_3), a secondary air pollutant, adversely impacts natural vegetation, agricultural crops, and human health (Feng et al., 2019; Lefohn et al., 2018). Despite China's implementation of stringent air pollution mitigation measures over the past decade (2014–2023), which reduced $PM_{2.5}$ concentrations in the Beijing-Tianjin-Hebei region by approximately 35 %, the 90th percentile of maximum daily 8-hour average O_3 concentrations (MDA8-O_3) have persistently stayed around of 180 μg m^{-3} (https://www.mee.gov.cn/). This concentration exceeds the safe limit of 100 μg m^{-3} which was 99th percentile of MDA8-O_3 and recommended by the World Health Organization (https://www.who.int/news-room/feature-stories/detail/what-are-the-

https://doi.org/10.5194/egusphere-2025-3956
Preprint. Discussion started: 12 September 2025
© Author(s) 2025. CC BY 4.0 License.

who-air-quality-guidelines). China is facing an increasingly prominent O_3 pollution problem. Developing effective strategies to mitigate O_3 pollution has become one of the most pressing environmental challenges in China (Wang et al., 2020).

O_3 formation is primarily associated with two precursors: VOCs and NO_x (Haagen-Smit, 1952). The fundamental pathways of O_3 formation comprise three sequential stages: (1) atmospheric oxidation of VOCs generates peroxy radicals (RO_2 and HO_2 radicals); (2) these radicals react with NO to form NO_2; and (3) photolytic decomposition of NO_2 produces O_3 (Bozem et al., 2017; Pusede et al., 2015). Considering the complex nonlinear relationship between O_3 formation and its precursors, O_3 control remains a persistent challenge in atmospheric environment. The sensitivity range of O_3 formation can be divided into three distinct regimes: (1) NO_x-limited regime, (2) VOC-sensitive regime, and (3) transitional regime with mixed precursors influence (Chu et al., 2024). However, the complex of atmospheric conditions hinders accurate characterization of chemical processes in models, resulting in significant biases in sensitivity analysis of O_3 formation (Li et al., 2018; Ma et al., 2021; Qu et al., 2021; Chen et al., 2024), and triggering debates over optimal precursor control strategies. Therefore, it is crucial to investigate the key factors influencing O_3 formation to provide a scientific basis for the prevention and control of O_3 pollution. Recent modeling studies have demonstrated that parameterization of ground mediated chemical processes enhances the simulation accuracy of O_3 production (Qin et al., 2025; Zhang et al., 2019). However, existing studies have predominantly focused on the heterogeneous conversion processes of NO_2 (Qin et al., 2025; Zhang et al., 2019), while the potential contributions of other ground mediated chemical reactions to O_3 production remain systematically unassessed probably due to the complex and diverse ground types.

Smog chamber has emerged as an indispensable approach for studying how secondary pollutants like O_3 formation (Chen et al., 2022; Pierce et al., 1995b). The smog chamber can simulate ambient atmospheric conditions under controlled meteorological settings. This allows for the study of physicochemical reactions while minimizing interference from meteorological variables. However, the chamber walls are not completely inert surfaces. Heterogeneous reactions may occur on these surfaces, accompanied by interfacial physical processes such as gas and aerosol adsorption/desorption (Pinho et al., 2005; Killus and Whitten, 1990; Chu et al., 2021), which will introduce biases into experimental data. Thus, it is necessary to consider the additional physicochemical mechanisms mediated by the chamber walls (wall effects) when analyzing chamber data.

The establishment of the Master Chemical Mechanism (MCM) relies heavily on smog chamber experiments (Wyche et al., 2010; Bloss et al., 2005), and its model systems serve as classical tools for simulating atmospheric O_3 formation (Shek et al., 2022; Wang et al., 2018; Liu et al., 2022). Toluene, as a typical anthropogenic VOC (Li et al., 2020) and isoprene, as a representative biogenic VOC (Guenther et al., 1995), both have high O_3 formation potential (Derwent et al., 1998). In our study, the smog chamber experimental results of toluene and isoprene mixed precursor systems were used as constraints for the MCM model to parametrize the wall effects allowing for the derivation of a revised model. And then, the influence of ground mediated reactions on the formation of O_3 was systematically explored by extrapolating the revised MCM model to

https://doi.org/10.5194/egusphere-2025-3956
Preprint. Discussion started: 12 September 2025
© Author(s) 2025. CC BY 4.0 License.

ambient atmospheric scenarios. Additionally, the simulation performance for O_3 in field was assessed by adjusting the ground surface heterogeneous reaction rate of NO_2, incorporating heterogeneous reactions of NO_2 on aerosol surfaces, and introducing an unknown sink for NO_2 within the model. The findings provide crucial theoretical foundation for precisely formulating prevention and control strategies targeting regional atmospheric O_3 pollution.

2 Experimental methods

The specific configuration and working principles of our 30 m^3 smog chamber system have been clearly described in our previous studies (Chen et al., 2019b; Chen et al., 2019a). To be brief, the rectangular chamber was made of FEP Teflon film with a thickness of 125 μm. A magnetic levitation fan is installed at the center of the bottom of the chamber to mix the reactants. The outside of the chamber is surrounded by stainless steel mirror panels, which are used to reflect ultraviolet light and make the irradiance uniform inside the chamber. One hundred and twenty ultraviolet lamps (Philips TL 60/10R) with a peak intensity of 365 nm are embedded in the stainless steel panels. After all the ultraviolet lamps are turned on, the photolysis rate of NO_2, used to characterize light intensity, was experimentally determined to be 0.0092 s^{-1} (Chen et al., 2022). And this is comparable to the light intensity at noon in Beijing. Before starting the experiment, the chamber was flushed with zero air at a flow rate of 100 L min^{-1} until the concentration of gas- and particle-phase contaminants is sufficiently low. An air conditioner is installed outside the chamber to control the reaction temperature, with an accuracy of ±1 ℃.

2.1 Smog chamber experiments

Toluene, isoprene and NO_x reserved in gas cylinders were introduced into the chamber using a mass flow controller. By precisely controlling the introduction time and flow rate, we managed to obtain precursor systems with different concentrations. The concentrations of toluene and isoprene were measured by a Vocus proton transfer reaction time-of-flight mass spectrometer (Vocus PTR-ToF-MS, Tofwerk AG, Aerodyne Research). The concentrations of NO_x and O_3 were measured using the NO−NO_2−NO_x analyzer (model 42i-TL, Thermo) and the O_3 analyzer (model 49i, Thermo), respectively.

Table 1: Detailed experimental conditions inside the smog chamber.

exp. no.[1]	RH (%)	T (°C)	$Isoprene_0$ (ppb)	$Toluene_0$ (ppb)	NO_0 (ppb)	$NO_{2,0}$ (ppb)	$NO_{x,0}$ (ppb)	(Isoprene+Toluene)/$NO_{x,0}$ (ppbC ppb^{-1})	ΔIsoprene (ppb)	ΔToluene (ppb)	ΔO_3 (ppb)
Iso&Tol01	53–62	28–30	11.52	11.31	25.08	0	24.58	5.56	9.82	2.14	45.56
Iso&Tol02	52–61	28–30	2.89	10.12	25.46	0	24.82	3.44	1.96	2.56	28.89
Iso&Tol03	53–62	28–30	11.70	1.43	26.06	0	25.03	2.74	9.90	0.12	30.02

https://doi.org/10.5194/egusphere-2025-3956
Preprint. Discussion started: 12 September 2025
© Author(s) 2025. CC BY 4.0 License.

Iso&Tol04	52–59	29–30	10.68	10.80	5.03	0.03	5.06	25.51	8.93	3.86	64.44
Iso&Tol05	52–61	28–30	8.26	6.31	1.01	0.27	1.28	66.78	7.30	1.60	51.61
Tol01	53–61	28–30	0[2]	10.95	25.38	0	24.61	3.18	0	4.10	22.95
Iso01	53–61	28–30	10.92	0	25.79	0	25.04	2.32	8.72	0	30.87
Iso02	52–64	27–30	13.16	0	26.29	0	25.43	2.70	10.89	0	34.93

[1]Iso represents isoprene, Tol represents toluene; [2]0 means that the relevant precursor was not added to the chamber.

Once all precursors concentration stabilized within the smog chamber, the fan was turned off, and the ultraviolet lamp was turned on to initiate the photochemical experiment, which persisted for a duration of 6 h. During the experiment, a temperature and humidity probe (Vaisala HMP110, Finland) was used to measure the temperature and relative humidity inside the chamber with a time resolution of 1 min. Fig. S1 and S2 reflect that the relative humidity and temperature were precisely regulated and maintained within the desired ranges during the experiments. The detailed experimental parameters are described in Table 1. According to the initial concentration ratios of VOCs and NO_x, the experiments covered three sensitivity regimes for O_3 formation.

2.2 The MCM box model (AtChem2)

AtChem2 model is constructed based on MCM: an explicit chemical mechanism. Although it does not take into account complex meteorological parameters, owing to its zero dimensional box model structure, it contains relatively complete atmospheric chemical reactions and enables rapid numerical simulation of atmospheric chemical processes. The core operation process of the model comprises the following key steps. Firstly, the initial concentrations of reactants, constraint conditions, and the chemical mechanism document are input. Subsequently, the coupled ordinary differential equations describing the chemical reactions in chemical mechanism document is compiled into Fortran executable code. Finally, the numerical integration algorithm for differential equations is employed to solve for the temporal evolution of the system variables. Detailed descriptions regarding the AtChem2 model have been reported in previous study (Cox et al., 2020).

In the smog chamber simulation, the NO_2 photolysis frequency, J_{NO_2}, was set to a constant value of 0.0092 s^{-1}, owing to the stable optical environment within the chamber. The calculation method of photolysis rates are provided as shown in Eq. (1) (Goliff et al., 2004; Borrás et al., 2024). By comparing the relationship between the experimental and calculated values of J_{NO_2}, the values of other photolysis rates in the model can be deduced (Carter et al., 1995a).

$$J = \int I(\lambda)\sigma(\lambda)\phi(\lambda)d\lambda \quad , \tag{1}$$

In the Eq. (1), the actinic flux I is used to characterize the distribution of light intensity within the smog chamber. The

https://doi.org/10.5194/egusphere-2025-3956
Preprint. Discussion started: 12 September 2025
© Author(s) 2025. CC BY 4.0 License.

absorption cross section σ and the quantum yield Φ describe the molecular light absorbing properties and energy conversion efficiency, respectively, during photolysis. The value of I is calculated based on the actual spectral data measured by the Miniature Fiber Optic Spectrometer as shown in Fig. S3. The parameters of σ and Φ are sourced from the MCM database. The final numerical settings of all the photolysis rate in the model are comprehensively presented in Table S1.

2.3 Description of observation site

The observation site is located on the campus of Beijing Institute of Petrochemical Technology in Daxing District, Beijing (39.73° N, 116.33° E) and the observation period was from 11 August 2019 to 19 August 2019. The details information about this site and measuring instruments can be found in our previous study (Chen et al., 2021; Xuan et al., 2023). Briefly, the observation platform is set on the top of the teaching building, approximately 27 m above the ground vertically. And the observation site is situated in the southern suburbs of Beijing, located in the northeastern part of the North China Plain. The surrounding environment of the observation point includes residential areas, educational institutions, and urban arterial roads. VOCs concentrations were quantified via vacuum ultraviolet single-photon ionization time-of-flight mass spectrometry (SPIMS-3000, Guangzhou Hexin Analytical Instrument Co., Ltd., China). The concentration of NO_x, SO_2, O_3, and CO was monitored using Thermo analyzers (Models 42i-TL, 43i, 49i, and 48i, respectively). HONO concentration was detected by a wet-chemical long-path absorption photometer (WLPAP, Zhichen Beijing) and the particle surface area concentration was derived from the scanning mobility particle sizer (SMPS, Model 3082 equipped with 3776 CPC, TSI Inc., USA). Additionally, the meteorological parameters (temperature, relative humidity, wind speed, wind direction and pressure) were recorded by an automatic weather station (Vaisala M451) and photolysis frequency of NO_2 (J_{NO_2}) was measured using a filter radiometer (Metcon GmbH, Germany). The time series of several representative parameters are shown in Fig. S5.

3 Results and discussion

3.1 Construction of a revised model accounting for chamber wall effects

Figure 1 presents the evolution of NO_x, O_3 and each VOC concentrations during the photochemical reaction systems with the mixed VOCs of toluene and isoprene. Two groups of typical experiments were selected to show the simulation results and improvement. For the experiment of Iso&Tol02, the initial ratio of VOCs to NO_x indicates that O_3 formation is under VOC-limited regime, and during which the photochemical processes can characterize the typical urban atmospheric environment. The experiment Iso&Tol04 is under NO_x-limited regime, corresponding to the atmospheric chemical characteristics of typical rural areas (Cheng et al., 2019). As shown in Fig. 1, there is a huge deviation between the simulation results of the basic model and the experimental values. For the Iso&Tol02 and Iso&Tol04 experiments, the NO_2 concentrations simulated by the basic model are significantly lower than the measured values. Considering that toluene is primarily consumed by oxidation with OH radicals, the degradation rate of toluene can reflect the concentration of OH radicals. However, the simulated degradation rates

https://doi.org/10.5194/egusphere-2025-3956
Preprint. Discussion started: 12 September 2025
© Author(s) 2025. CC BY 4.0 License.

of toluene by basic model are considerably lower than the measured values (Fig. 1e and 1j), suggesting that there is a huge gap between the simulated and actual concentrations of OH radicals. For the Iso&Tol02 and Iso&Tol04 experiments, the O_3 values simulated by the basic model are lower than the measured values, with NMB values of -83.9 % and -41.3 %, respectively. The calculation method of NMB is detailed in Section S1. The significant discrepancy between simulations and measurements lies in the model's failure to account for wall related reaction mechanisms. Identifying these reactions and incorporating their parameterization into the model is therefore imperative.

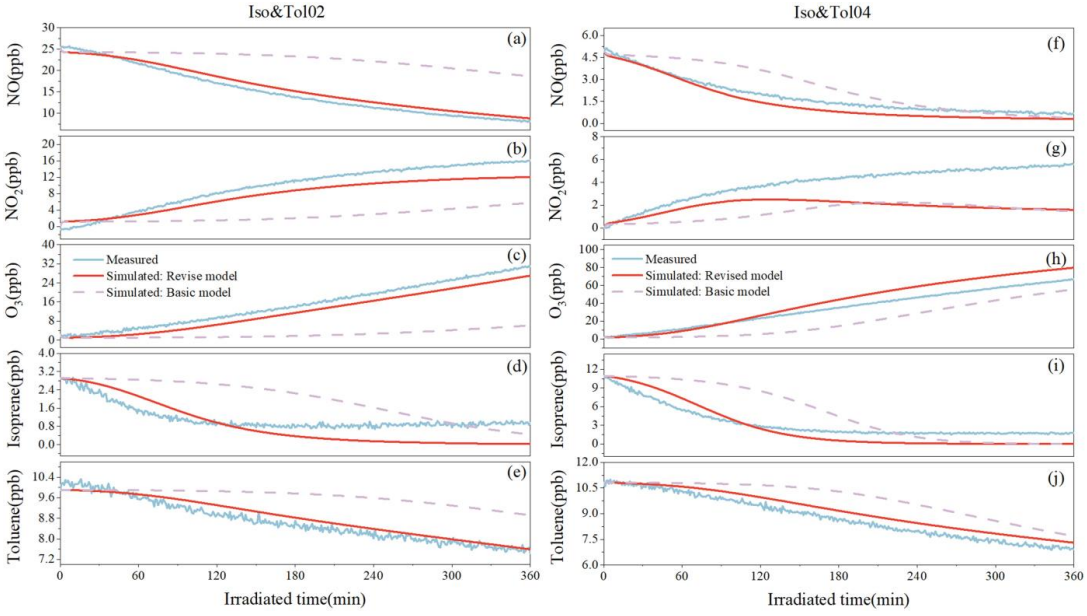

Figure 1: Time series of (a, f) NO, (b, g) NO_2, (c, h) O_3, (d, i) isoprene and (e, j) toluene during the photochemical reaction process in experiments of Iso&Tol02 and Iso&Tol04. The blue line represents the measured values, the red line denotes the simulation results of the revised model, and the dashed line indicates the simulation results of the basic model. The NMB values for O_3 simulated by the basic model, revised model in experiment Iso&Tol02 were -83.9 % and -19.0 %, respectively. And that in experiment Iso&Tol04 were -41.3 % and 20.0 %, respectively.

Currently, numerous studies have investigated the chamber wall effects and determined the corresponding reaction rate constants (Lurmann et al., 1991; Bloss et al., 2005; Metzger et al., 2008; Wang et al., 2014). Table 2 summarizes the reactions related to the wall effects and their reaction rate constants used in our study. The wall photogenerated OH radicals mechanism is incorporated into the model to bridge the discrepancy between simulated and measured values. The feasibility of this mechanism has been verified in the studies conducted by Angove et al. (2005). and Lurmann et al. (1991). In order to better simulate the degradation trend of VOCs, the optimal generation rate constant of OH radicals in the model is determined to be 1.2×10^6 molecules cm^{-3} s^{-1}, which is close to the findings of Wang et al. (2014). Meanwhile, the mechanism of light-induced

https://doi.org/10.5194/egusphere-2025-3956
Preprint. Discussion started: 12 September 2025
© Author(s) 2025. CC BY 4.0 License.

release of NO_2 from the wall (Bloss et al., 2005; lurmann et al., 1991) was introduced to address the issue of relatively low production of NO_2 in the simulation. The determined optimal release rate constant of NO_2 is 6×10^5 molecules cm^{-3} s^{-1}, falling between the results reported by Angove et al. (2005) and Wang et al. (2014). In addition, Teflon wall can release small amounts of organic impurities, which will consume OH radicals and generate HO_2 radicals (Metzger et al., 2008). Therefore, the additional mechanism that converts OH radicals into HO_2 radicals was also introduced into the model. This mechanism can accelerate the consumption of NO and also compensating for the deficiency of the simulated NO_2 and O_3 concentration. The optimal conversion rate constant of OH radicals to HO_2 radicals is determined to be 10 s^{-1}, which lies within the range mentioned by Lurmann et al. (1991).

Table 2: The additional mechanisms related to wall effects and their associated reaction rate parameters.

	Additional mechanisms	Parameter	Notes
1	hν + wall → OH	1.2×10^6 molecule cm^{-3} s^{-1}	Refered to Angove et al. (2005)
2	hν + wall → NO_2	6×10^5 molecule cm^{-3} s^{-1}	Refered to Angove et al. (2005)
3	OH → HO_2	10 s^{-1}	Refered to Lurmann et al. (1991)
4	N_2O_5 → 2wHNO_3[1]	1×10^{-5} s^{-1}	Adopted from Bloss et al. (2005)
5	N_2O_5 + H_2O → 2wHNO_3	1×10^{-20} cm^3 s^{-1}	Adopted from Bloss et al. (2005)
6	HNO_3 → wHNO_3	1×10^{-4} s^{-1}	Adopted from Bloss et al. (2005)
7	NO_2 → 0.5HONO + 0.5wHNO_3	1×10^{-6} s^{-1}	Adopted from Angove et al. (2005)
8	wHNO_3 + hν → OH + NO_2	J_{wHNO_3}	Theoretical calculation
9	O_3 → wall	5.53×10^{-6} s^{-1}	Chamber characterization/measured

[1]wHNO_3 represents adsorbed HNO_3 on the wall.

In addition, the heterogeneous reactions and homogeneous hydrolysis of N_2O_5, the wall losses of HNO_3 and O_3, the photolysis of wHNO_3 as well as the heterogeneous reactions of NO_2 have also been considered as wall related reaction mechanisms (Metzger et al., 2008; Bloss et al., 2005). These reactions need to be incorporated into the model. The rate constants of the heterogeneous reaction and homogeneous hydrolysis of N_2O_5 are set at 1×10^{-5} s^{-1} and 1×10^{-20} cm^3 s^{-1}, respectively. The wall loss rate constant of HNO_3 is taken as 1×10^{-4} s^{-1}. These values are consistent with the studies of Metzger et al. (2008) and Angove et al. (2005). The rate constant of the heterogeneous reaction of NO_2 is set at 1×10^{-6} s^{-1}, which is in line with the research of Angove et al. (2005). The photolysis rate constant of wHNO_3 is assumed to be the same as that of gaseous HNO_3 and is calculated to be 5.66×10^{-7} s^{-1} by the Eq. (1). The wall loss rate constant of O_3 is experimentally determined

https://doi.org/10.5194/egusphere-2025-3956
Preprint. Discussion started: 12 September 2025
© Author(s) 2025. CC BY 4.0 License.

to be 5.53×10^{-6} s^{-1}. After introducing additional mechanisms, a revised model has been developed.

3.2 The performance evaluation of the revised model

As shown in Fig. 1, after applying the revised model, the simulation accuracy of each experimental parameter has been significantly improved. The NMB of O_3 in experiment of Iso&Tol02 increased significantly from -83.9 % to -19.0 %, and that in experiment of Iso&Tol04 increased from -41.3 % to 20.0 %. The simulation performance of O_3 concentrations in other experiments was also significantly improved. In experiments of Iso&Tol01, Iso&Tol03, Iso&Tol05, Tol01, Iso01, Iso02, the NMB of O_3 changed from -91.1 % to -3.8 %, -83.9 % to -12.5 %, -56.9 % to -26.6 %, -81.9 % to -13.8 %, -84.4 % to -24.1 %, and -85.7 % to -21.6 %, respectively as shown in Fig. S4. Following the implementation of the revised model, the NMB of all experiments are distributed within the range of from -26.6 % to 20.0 %, with an average of -12.7 %. Consequently, the revised model substantially reduced the discrepancies between simulated and observed values for key experiment parameters compared to the basic model, establishing a basis for subsequent sensitivity analysis.

3.3 Impact of the revised model on the sensitivity of O_3 formation in smog chamber compared to the basic model

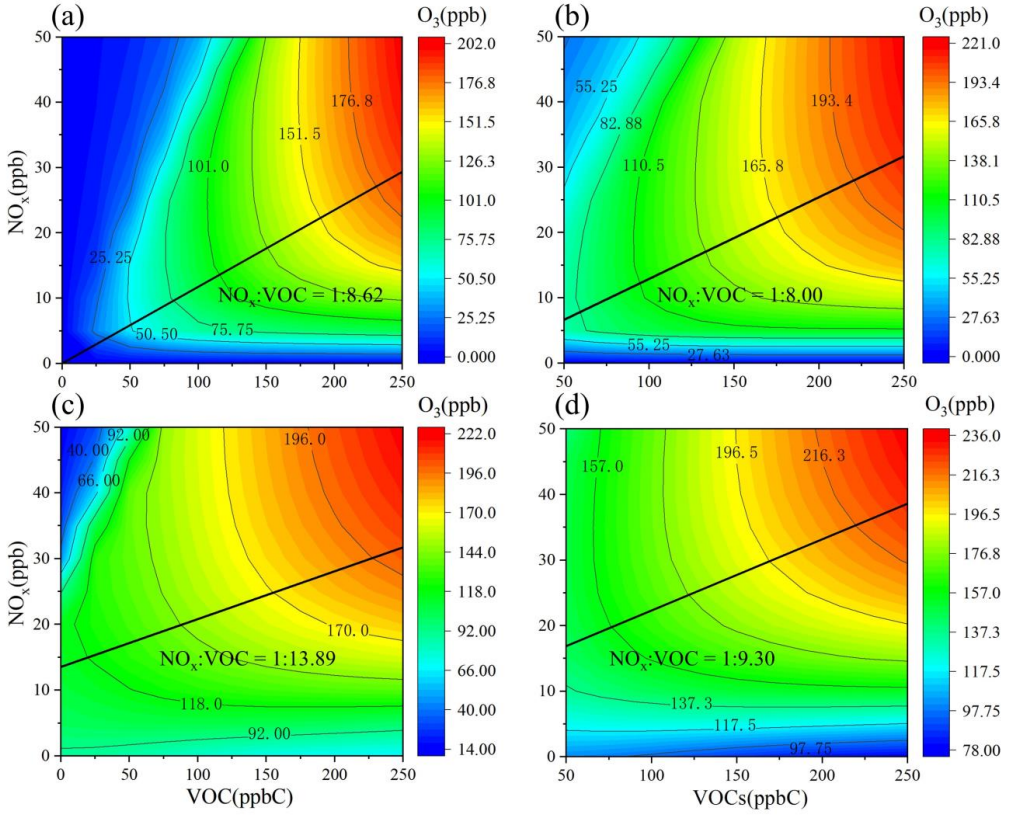

Figure 2: Simulated EKMA curves for O_3 generation under the (a) toluene only system and (b) mixed VOCs system using the basic

https://doi.org/10.5194/egusphere-2025-3956
Preprint. Discussion started: 12 September 2025
© Author(s) 2025. CC BY 4.0 License.

model. Correspondingly, (c) and (d) display the simulated EKMA curves for O_3 generation under the toluene only system and mixed VOCs system, respectively using the revised model.

In order to determine the specific impacts of the revised model on the sensitivity of O_3 formation, the EKMA (Empirical Kinetic Modeling Approach) curves were obtained by simulating O_3 formation under varying concentration of VOCs and NO_x (Liu et al., 2022; Ma et al., 2021). As illustrated in Fig. 2, the simulation results demonstrated the nonlinear response characteristics of O_3 production to precursors. Meanwhile, it can be found that, whether in the toluene only system or in the toluene isoprene mixed system, the slope of the ridge line of the EKMA curves derived from the revised model changes. This indicates that the model revision alters the sensitivity of O_3 formation to its precursors. Therefore, it is necessary to incorporate mechanisms related to wall effects into the model to accurately capture the O_3 formation sensitivity. Comparing scenarios with and without isoprene (Fig. 2d and 2c), the results showed that the slope of the EKMA ridge line increases (1:13.89 vs. 1:9.30) when isoprene are considered, further emphasizing the necessity of stringent NO_x control for effective O_3 pollution mitigation. Consequently, to establish a more accurate precursor response relationship, it is essential to account for the contribution of biogenic VOCs (such as isoprene) in the model. This conclusion is also supported by the findings of Tan et al. (2018).

3.4 The impact of the revised model that accounts for surface-to-volume ratio on the atmospheric O_3 formation compared to the basic model

The applicability of the revised model under atmospheric conditions was further investigated. Due to the difference in surface-to-volume ratio between the atmospheric environment and smog chamber, the rate constants related to surface reactions should be adjusted when applying the revised model to the ambient atmosphere. To facilitate the study of atmospheric O_3 formation sensitivity in a zero dimensional box model, the boundary layer height was assumed to be ranged from 300 m at night to 1500 m in the afternoon throughout the simulations (Gao et al., 2014; Xuan et al., 2024; Wang et al., 2025), and the atmospheric surface-to-volume ratio was calculated using Eq. (3) (Li et al., 2010). Assuming that the uptake coefficient in the chamber wall is equal to that in the atmospheric ground, the ground related reaction rate constant can be derived using Eq. (2), which presents the calculation method for the heterogeneous reaction rate constant of HONO (Gao et al., 2014).

$$k = \frac{1}{8}\gamma \mathrm{v}_{\mathrm{NO_2}} \frac{\mathrm{S}}{V_\mathrm{g}} , \quad (2)$$

$$\frac{\mathrm{S}}{\mathrm{V_g}} = \frac{1.7}{\mathrm{H}} , \quad (3)$$

where k is defined as the surface reaction rate constant for HONO, γ represents the uptake coefficient, $\mathrm{v}_{\mathrm{NO_2}}$ denotes the average molecular velocity of NO_2, and S/V_g stands for the surface-to-volume ratio of the ground. H denotes the boundary layer height.

https://doi.org/10.5194/egusphere-2025-3956
Preprint. Discussion started: 12 September 2025
© Author(s) 2025. CC BY 4.0 License.

Specifically, the surface reaction rate constant in the ambient atmosphere at night and in the afternoon can be obtained by multiplying the corresponding values in the chamber by 2.9×10^{-3} and 5.8×10^{-4}, respectively. In the further revised model, the surface reaction rate constants were adjusted in the manner described above to develop an atmospheric relevant revised model that accounts for surface-to-volume ratio, named SVR model. This parameterization strategy specifically addresses surface mediated kinetic disparities between smog chamber and atmospheric environment.

In the SVR model and basic model, the observed species concentrations and meteorological parameters are constrained. Inorganic pollutants include NO, SO_2 and CO, while meteorological parameters encompass temperature, relative humidity, atmospheric pressure, and the photolysis rate of NO_2. Considering both the operational efficiency and the accuracy of simulations, the top 20 VOCs with the highest maximum incremental reactivity (MIR) values are selected for constraint (Carter, 2009). Detailed information on the constrained species can be found in Table S2. It should be noted that we did not constrain NO_2 and HONO. Additional mechanisms in Table 2 involve the source and sink processes of NO_2. Constraining NO_2 in the model will weaken the research significance of the revised model. HONO serves as a significant source of OH radicals in the atmospheric environment, exerting a critical influence on O_3 formation. Moreover, its source–sink processes are closely linked to NO_x, meaning that constraining HONO could hinder the analysis of O_3 reduction scenarios.

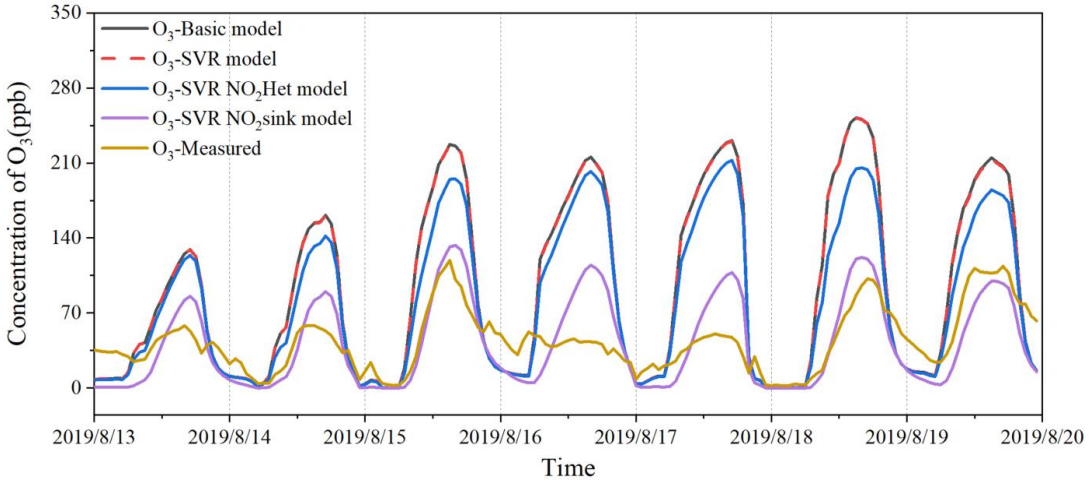

Figure 3: Measured concentrations of O_3 and the simulation results of different models in Daxing, Beijing from 13–19 August 2019. The NMB values for O_3 simulated by the basic model, SVR model, SVR NO_2Het model, and SVR NO_2sink model were 113.8 %, 113.0 %, 84.1 % and -5.2 %, respectively.

Unexpectedly, the simulation results of SVR model and basic model showed minimal differences (Fig. 3). It is speculated that this is due to the too small surface-to-volume ratio (5.7×10^{-3}–1.1×10^{-3}) of the ground, resulting in weak influence of ground related reactions on atmospheric chemistry. Meanwhile, the simulated O_3 concentrations of both models are far higher

https://doi.org/10.5194/egusphere-2025-3956
Preprint. Discussion started: 12 September 2025
© Author(s) 2025. CC BY 4.0 License.

than the measured values, with calculated NMB values of 113.0 % and 113.8 %, respectively. The simulated NO_2 concentrations of both models also significantly exceed the measured values as seen in Fig. S6, with NMB values of 536.7 % and 539.8 %, respectively. And the simulated HONO concentrations were far lower than the measured values, with the NMB values being -94.3 % and -94.8 %, respectively as seen in Fig. S7. These findings indicate that the atmospheric environment is more complex than smog chambers, due to additional chemical reactions influencing O_3 formation. To obtain accurate O_3 formation sensitivity, the model requires further revision.

3.5 Further revision of models for complex atmospheric environments

An important sink of NO_2 is its heterogeneous reactions on ground surface and aerosol surface in the atmosphere (Liu et al., 2019; Xuan et al., 2024). The fact that the SVR model underestimates the ground level reaction rate of NO_2 and neglects its heterogeneous reactions on aerosol surface is likely the major reason for the overestimation of simulated NO_2 concentrations, which in turn leads to the overestimation of simulated O_3 levels. Table 3 summarizes the equations for NO_2 heterogeneous reactions and the calculation methods for their rate constants.

Table 3: Parametrization of heterogeneous reactions in AtChem2-MCM.

Heterogeneous reaction	Rate constant	Uptake coefficient	Notes
$2NO_2$ + ground surface → HONO + HNO_3	$k_{gn} = \frac{1}{8} \times \gamma_g \times \nu_{NO_2} \times \frac{1.7}{H}$	$\gamma_g = 8\times10^{-6}$	Adopted from Liu et al. (2019)
$2NO_2$ + ground surface + $h\nu$ → HONO	$k_{gd} = \frac{1}{8} \times \gamma_{gd} \times \nu_{NO_2} \times \frac{1.7}{H} \times \frac{J_{NO_2}}{0.007s^{-1}}$	$\gamma_{gd} = 6\times10^{-5}$	Adopted from Liu et al. (2019)
$2NO_2$ + aerosol surface → HONO + HNO_3	$k_{an} = \frac{1}{4} \times \gamma_a \times \nu_{NO_2} \times S_a$	$\gamma_a = 8\times10^{-6}$	Adopted from Liu et al. (2019)
$2NO_2$ + aerosol surface + $h\nu$ → HONO	$k_{ad} = \frac{1}{4} \times \gamma_{ad} \times \nu_{NO_2} \times S_a \times \frac{J_{NO_2}}{0.007s^{-1}}$	$\gamma_{ad} = 1\times10^{-3}$	Adopted from Liu et al. (2019)
NO_2 → product	$k_{NO_2} = 1.5\times10^{-4}\ s^{-1}$		

γ_g and γ_a denote the uptake coefficients of NO_2 on ground surface and aerosol surface, respectively, while γ_{gd} and γ_{ad} represent the photo-enhanced uptake coefficients of NO_2 under illuminated conditions for ground and aerosol surfaces, respectively.

As shown in Fig. 3, after incorporating these heterogeneous reactions of NO_2 into the model (Named SVR NO_2Het model), the simulation performance for O_3 improved, with an NMB value of 84.1 %. And the simulation performance of NO_2 has also been enhanced as shown in Fig. S6, with an NMB value of 436.7 %. However, the simulated values of HONO were far higher

https://doi.org/10.5194/egusphere-2025-3956
Preprint. Discussion started: 12 September 2025
© Author(s) 2025. CC BY 4.0 License.

than the measured ones as shown in Fig. S7. Significant discrepancies still exist between the simulated and measured results, indicating that some unidentified sinks of NO_2 have yet to be accounted for. Building on this, a constant sink of NO_2 was incorporated into the model (Named SVR NO_2sink model), leading to a substantial improvement in O_3 simulation performance (Fig. 3), with a NMB value of -5.2 %. The simulation performance of NO_2 and HONO also demonstrated notable accuracy, achieving NMB values of -13.3 % and -12.4 %, respectively as shown in Fig. S6 and S7. As presented in Fig. S8, the simulated concentrations of OH and HO_2 radicals reached peak values of 1.20×10^7 and 1.23×10^9 molecules cm^{-3} s^{-1}, respectively. These magnitudes are comparable to observations and model results reported for Beijing in previous studies (Slater et al., 2021; Chai et al., 2023). However, the O_3 simulated levels for 16–17 August were significantly higher than the observed values. This discrepancy can be attributed to the prevailing westerly winds starting from the 15 August (Fig. S5), which led to a change in air masses and a significant decrease in NO_2 concentrations in the atmosphere. This change was not captured by the zero dimensional box model, resulting in a substantial overestimation of O_3 concentrations. In conclusion, the simulation results confirm the existence of unidentified NO_2 sinks in the atmospheric environment. Zheng et al. (2024) have shown that the ionic strength in aerosol liquid water can enhance the uptake coefficient of NO_2 on aerosol surface and the reaction rate constant for NO_2 they adopted in the field simulation is approximately on the order of 10^{-6} s^{-1}. Furthermore, evidence from Chu et al. (2023) validates the mechanism of photo-enhanced heterogeneous reactions of NO_2 on building surfaces and their simulation results indicated that the reaction rate constant of NO_2 related to N_2O_5 was on the order of 10^{-6} s^{-1}. However, these NO_2 reaction rate constants were significantly lower than the artificially high values adopted in our model (see Table 3), and to our knowledge, no previous studies have reported the rate constant of such magnitude in atmospheric environment. The reactions associated with NO_2 sinks under the complex atmospheric environments require further investigation.

3.6 Impact of model revision on O_3 formation sensitivity in the atmosphere

EKMA curves of O_3 formation in Daxing District of Beijing were obtained by designing multiple sets of reduction scenarios under basic model and SVR NO_2sink model, as shown in Fig. 4. Given that biogenic sources of VOCs are difficult to control, only reductions in concentrations of anthropogenic VOCs (AVOCs) were considered in designing VOCs reduction scenarios. These results demonstrate that both models consistently indicated that O_3 formation in Daxing District of Beijing during summer is more sensitive to VOCs than to NO_x, aligning with findings from previous studies conducted in Beijing (Chai et al., 2023; Han et al., 2023). However, a comparative analysis of model simulations revealed significant discrepancies between the basic model and the SVR NO_2sink model in predicting O_3 formation in Daxing District of Beijing. The simulated O_3 values from the basic model are far higher than those from the SVR NO_2sink model. Furthermore, the ridge line slope derived from the EKMA curve of the basic model (1:2.41) is lower than that from the SVR NO_2sink model (1:2.06). These findings collectively indicated that the basic model not only overestimated actual ambient O_3 levels but also distorted the non-linear relationship between O_3 and its precursors, potentially misleading formulation of emission reduction policies. In contrast, the

https://doi.org/10.5194/egusphere-2025-3956
Preprint. Discussion started: 12 September 2025
© Author(s) 2025. CC BY 4.0 License.

predictions of O_3 concentrations by SVR NO_2sink model are closer to observed values and, critically, its steeper ridge line slope indicated that the sensitivity of O_3 to VOCs in Daxing has been enhanced. When NO was constrained and additional NO_2 sinks were considered in the model, the proportion of NO in NO_x would increase. Elevated NO levels reduce the relative importance of NO in its reactions with HO_2 and RO_2 radicals, thereby increasing the significance of these radicals, which are key oxidation products of VOCs. Therefore, adding extra NO_2 sinks in the model makes O_3 formation more sensitive to VOCs. Considering the Class I ambient air quality standard for O_3 in China (1-hour average: ~80 ppb), the results from SVR NO_2sink model demonstrated that meeting the O_3 target requires either roughly a 76 % reduction in NO_x by itself, or about a 60 % reduction in VOCs by itself. But when reducing both two pollutants in coordination, a lower reduction ratio (53 % for NOx and 46 % for VOCs, respectively) can achieve compliance requirements. Simulated emission reduction scenarios reveal VOCs control is a higher priority over NO_x reduction in achieving O_3 abatement targets for Daxing. The above content underscores the critical importance of incorporating atmospheric NO_2 sinks into the box model for formulating scientific policies on O_3 emission reduction. A deeper investigation into the dominant atmospheric sinks of NO_2 is fundamentally important.

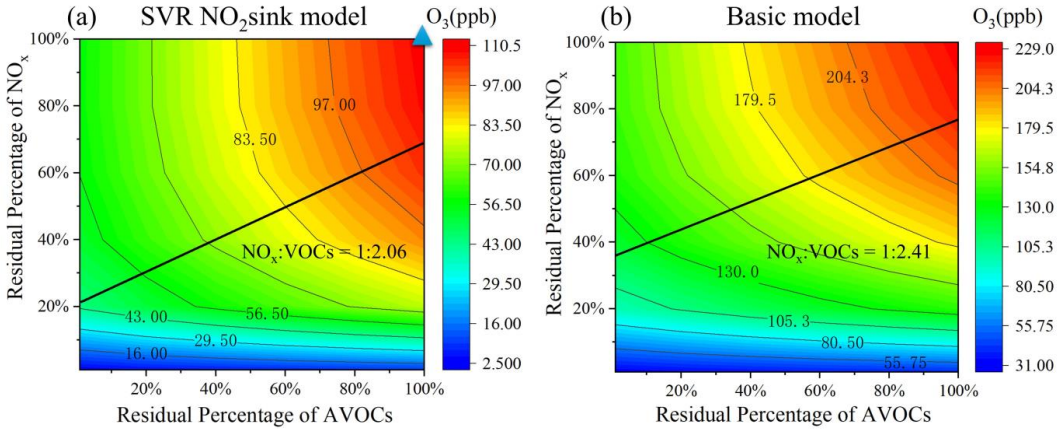

Figure 4: Simulated O_3 EKMA curves based on (a) SVR NO_2sink model and (b) basic model in Daxing District during 13–19 August 2019. The triangular marker in the upper right corner of the (a) denotes the O_3 formation scenario before emission reduction.

4 Conclusions and implications

Our study significantly improved the understanding of the response relationship between atmospheric O_3 and its precursors through smog chamber experiments and box model revisions, and revealed the critical influence of the unidentified NO_2 sink on O_3 sensitivity analysis. By incorporating reactions associated with the chamber wall into the box model, the simulation performance for O_3 formation in smog chamber was markedly improved, with the average NMB reduced from −76.1 % to

https://doi.org/10.5194/egusphere-2025-3956
Preprint. Discussion started: 12 September 2025
© Author(s) 2025. CC BY 4.0 License.

−12.7 %. This improvement arises because such wall-related processes influence both the generation and elimination of OH radicals and the evolution of reactive nitrogen in the system, mainly including the release of OH radicals, the consumption of OH radicals by residual organics on the wall, and the heterogeneous reactions of NO_2, N_2O_5, and HNO_3. When applying the chamber-derived model to summer O_3 formation in Beijing's Daxing District, field-specific revisions were necessary. The most critical was adding an unidentified NO_2 sink. Incorporating this sink and other adjustments markedly improved performance, reducing NMB from 113.8 % to –5.2 % except for a few days influenced by air mass changes. Sensitivity analysis indicated an enhanced dependence of O_3 formation on VOC control in Daxing District. The introduction of the NO_2 sink accelerated NO_2 removal, weakened the scavenging effect of NO_x on HO_2 and RO_2, thereby increasing radical concentrations and promoting VOC-driven O_3 production. This mechanism explains the shift in sensitivity regime, thereby highlighting the important regulatory role of NO_2 sink analysis in regional photochemical processes. This method can be extended to other regions following the steps illustrated in Figure 5, offering a scientific basis for developing regional O_3 pollution prevention and control strategies.

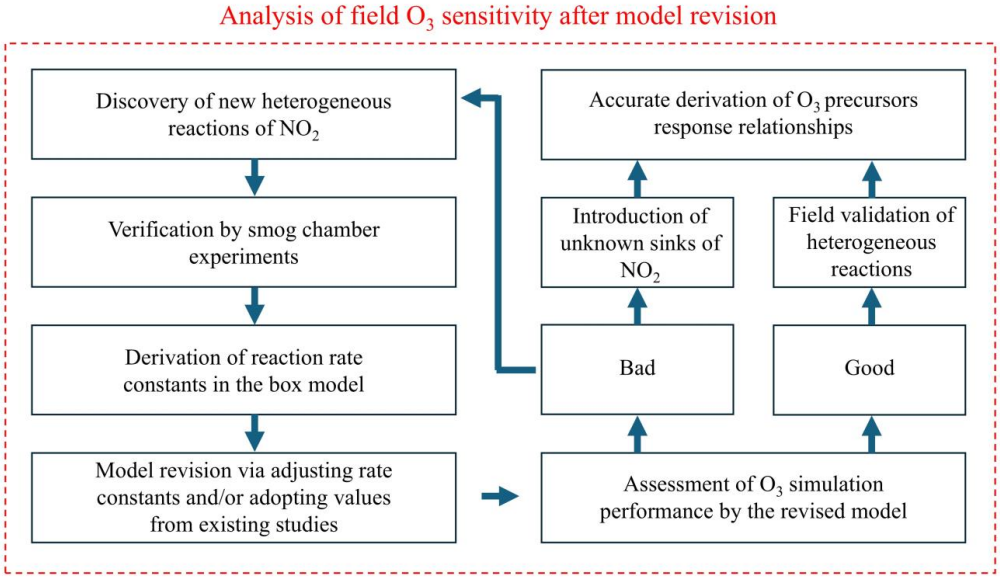

Figure 5: Schematic illustration of methods for accurately obtaining O_3 precursors response relationships.

Multiple studies employing different approaches have examined the sensitivity of O_3 formation in Beijing, consistently finding that O_3 production in the region is primarily VOC-limited (Cui et al., 2021; Nelson et al., 2024; Ji et al., 2025). This conclusion aligns with the diagnostic results of the present study, indirectly validating the reliability of the simulations. It should be noted, however, that the NO_2 sink used in this study exceeds levels reported in previous studies (Chu et al., 2023; Zheng et al., 2024). While this may lead to an overestimation of the magnitude of sensitivity changes, such a sink is still likely

https://doi.org/10.5194/egusphere-2025-3956
Preprint. Discussion started: 12 September 2025
© Author(s) 2025. CC BY 4.0 License.

to occur under complex atmospheric environment. Moreover, the zero-dimensional box model does not fully account for meteorological factors and does not consider the influence of regional transport, which may affect the applicability of the results. Further systematic studies on NO_2 sinks are urgently needed to better simulate O_3 formation.

Code and data availability. The observation data at this site are available from the authors upon request.

Supplement. The supplement will be published alongside this article.

Author contributions. Conceptualization: BWC; Data curation: TZC, JL and HYX; Formal analysis: JLL; Funding acquisition: TZC and BWC; Investigation: JLL; Methodology: BWC, TZC and JLL; Resources: HH; Writing (original draft preparation): JLL and TZC; Writing (review and editing): TZC, BWC, JL, HYX, PZ, QXM, YHW and HL.

Competing interests. The authors declare that they have no conflict of interest.

Acknowledgments. The authors thank all the workers who provided support during this field observation period.

Financial support. This work was financially supported by the National Key Research and Development (R&D) Program of China (2024YFC3714300), the National Natural Science Foundation of China (22376206 and 22188102), and the Youth Innovation Promotion Association, CAS (Y2022023 and Y2022021).

Review statement.

References

Angove, D. E., Hynes, R. G., Saunders, S. M., Haverd, V., and Azzi, M.: Evaluation of two MCM v3.1 alkene mechanisms using indoor environmental chamber data, Atmospheric Environment, 39, 7251-7262, https://doi.org/10.1016/j.atmosenv.2005.09.005, 2005.

Bloss, C., Wagner, V., Bonzanini, A., Jenkin, M. E., Wirtz, K., Martin-Reviejo, M., and Pilling, M. J.: Evaluation of detailed aromatic mechanisms (MCMv3 and MCMv3.1) against environmental chamber data, Atmos. Chem. Phys., 5, 623-639, 10.5194/acp-5-623-2005, 2005.

Borrás, E., Löher, F., Muñoz, A., and Nölscher, A. C.: Characterization of a new Teflon chamber and on-line analysis of isomeric multifunctional photooxidation products, Atmospheric Measurement Techniques, 17, 4553-4579, https://amt.copernicus.org/articles/17/4553/2024/, 2024.

Butler, T. M., Bozem, H., Lawrence, M. G., Harder, H., Martinez, M., Kubistin, D., Lelieveld, J., and Fischer, H.: Chemical processes related to net ozone tendencies in the free troposphere, Atmos. Chem. Phys., 17, 10565-10582, 10.5194/acp-17-10565-2017, 2017.

Carter, W., Luo, D., Malkina, I., and Pierce, J.: Environmental chamber studies of atmospheric reactivities of volatile organic

https://doi.org/10.5194/egusphere-2025-3956
Preprint. Discussion started: 12 September 2025
© Author(s) 2025. CC BY 4.0 License.

compounds. Effects of varying chamber and light source, National Renewable Energy Lab.(NREL), Golden, CO (United States), https://intra.cert.ucr.edu/~carter/pubs/explrept.pdf, 1995a.

Carter, W. P.: Updated maximum incremental reactivity scale and hydrocarbon bin reactivities for regulatory applications, California Air Resources Board Contract, 339, https://ww2.arb.ca.gov/sites/default/files/barcu/regact/2009/mir2009/mir10.pdf, 2009.

Chai, W., Wang, M., Li, J., Tang, G., Zhang, G., and Chen, W.: Pollution characteristics, sources, and photochemical roles of ambient carbonyl compounds in summer of Beijing, China, Environmental Pollution, 336, 122403, https://doi.org/10.1016/j.envpol.2023.122403, 2023.

Chen, G., Xu, L., Yu, S., Xue, L., Lin, Z., Yang, C., Ji, X., Fan, X., Tham, Y. J., Wang, H., Hong, Y., Li, M., Seinfeld, J. H., and Chen, J.: Increasing Contribution of Chlorine Chemistry to Wintertime Ozone Formation Promoted by Enhanced Nitrogen Chemistry, Environmental Science & Technology, 58, 22714-22721, 10.1021/acs.est.4c09523, 2024.

Chen, T., Chu, B., Ge, Y., Zhang, S., Ma, Q., He, H., and Li, S.-M.: Enhancement of aqueous sulfate formation by the coexistence of NO_2/NH_3 under high ionic strengths in aerosol water, Environmental Pollution, 252, 236-244, https://doi.org/10.1016/j.envpol.2019.05.119, 2019a.

Chen, T., Liu, Y., Ma, Q., Chu, B., Zhang, P., Liu, C., Liu, J., and He, H.: Significant source of secondary aerosol: formation from gasoline evaporative emissions in the presence of SO_2 and NH_3, Atmos. Chem. Phys., 19, 8063-8081, 10.5194/acp-19-8063-2019, 2019b.

Chen, T., Liu, J., Ma, Q., Chu, B., Zhang, P., Ma, J., Liu, Y., Zhong, C., Liu, P., Wang, Y., Mu, Y., and He, H.: Measurement report: Effects of photochemical aging on the formation and evolution of summertime secondary aerosol in Beijing, Atmos. Chem. Phys., 21, 1341-1356, 10.5194/acp-21-1341-2021, 2021.

Chen, T., Zhang, P., Ma, Q., Chu, B., Liu, J., Ge, Y., and He, H.: Smog Chamber Study on the Role of NO_x in SOA and O_3 Formation from Aromatic Hydrocarbons, Environmental Science & Technology, 56, 13654-13663, 10.1021/acs.est.2c04022, 2022.

Cheng, N., Li, R., Xu, C., Chen, Z., Chen, D., Meng, F., Cheng, B., Ma, Z., Zhuang, Y., He, B., and Gao, B.: Ground ozone variations at an urban and a rural station in Beijing from 2006 to 2017: Trend, meteorological influences and formation regimes, Journal of Cleaner Production, 235, 11-20, https://doi.org/10.1016/j.jclepro.2019.06.204, 2019.

Chu, B., Chen, T., Liu, Y., Ma, Q., Mu, Y., Wang, Y., Ma, J., Zhang, P., Liu, J., Liu, C., Gui, H., Hu, R., Hu, B., Wang, X., Wang, Y., Liu, J., Xie, P., Chen, J., Liu, Q., Jiang, J., Li, J., He, K., Liu, W., Jiang, G., Hao, J., and He, H.: Application of smog chambers in atmospheric process studies, National Science Review, 9, 10.1093/nsr/nwab103, 2021.

Chu, B., Liu, Y., Li, H., Jia, Y., Liu, J., Cao, Q., Chen, T., Zhang, P., Ma, Q., Zeng, X. C., Francisco, J. S., and He, H.: Photocatalytic Oxidation of NO_2 on TiO_2: Evidence of a New Source of N_2O_5, Angewandte Chemie, 135, e202304017, https://doi.org/10.1002/ange.202304017, 2023.

Chu, W., Li, H., Ji, Y., Zhang, X., Xue, L., Gao, J., and An, C.: Research on ozone formation sensitivity based on observational methods: Development history, methodology, and application and prospects in China, Journal of Environmental Sciences, 138, 543-560, https://doi.org/10.1016/j.jes.2023.02.052, 2024.

Cox, S., Sommariva, R., Martin, C., Borońska, K., Young, J., Jimack, P. K., Pilling, M. J., Matthaios, V. N., Nelson, B. S., Newland, M. J., Panagi, M., Bloss, W. J., Monks, P. S., and Rickard, A. R.: AtChem (version 1), an open-source box model for the Master Chemical Mechanism, Geosci. Model Dev., 13, 169-183, 10.5194/gmd-13-169-2020, 2020.

Cui, M., An, X., Xing, L., Li, G., Tang, G., He, J., Long, X., and Zhao, S.: Simulated Sensitivity of Ozone Generation to Precursors in Beijing during a High O_3 Episode, Advances in Atmospheric Sciences, 38, 1223-1237, 10.1007/s00376-021-0270-4, 2021.

Derwent, R. G., Jenkin, M. E., Saunders, S. M., and Pilling, M. J.: Photochemical ozone creation potentials for organic compounds in northwest Europe calculated with a master chemical mechanism, Atmospheric Environment, 32, 2429-2441, https://doi.org/10.1016/S1352-2310(98)00053-3, 1998.

Feng, Z., De Marco, A., Anav, A., Gualtieri, M., Sicard, P., Tian, H., Fornasier, F., Tao, F., Guo, A., and Paoletti, E.: Economic losses due to ozone impacts on human health, forest productivity and crop yield across China, Environment International, 131, 104966, https://doi.org/10.1016/j.envint.2019.104966, 2019.

https://doi.org/10.5194/egusphere-2025-3956
Preprint. Discussion started: 12 September 2025
© Author(s) 2025. CC BY 4.0 License.

Gao, J., Xue, L. K., Wang, T., Ding, A. J., Zhou, X. H., Blake, D. R., Wang, X. F., Saunders, S. M., Fan, S. J., Zuo, H. C., Zhang, Q. Z., and Wang, W. X.: Ground-level ozone in four Chinese cities: precursors, regional transport and heterogeneous processes, Atmos. Chem. Phys., 14, 13175-13188, 10.5194/acp-14-13175-2014, 2014.

Goliff, W. S. and Stockwell, W. R.: Measurement of actinic flux and the calculation of photolysis rate parameters for the Central California Ozone Study, Atmospheric Environment, 38, 5169-5177, https://www.sciencedirect.com/science/article/abs/pii/S1352231004005114, 2004.

Guenther, A., Hewitt, C. N., Erickson, D., Fall, R., Geron, C., Graedel, T., Harley, P., Klinger, L., Lerdau, M., Mckay, W. A., Pierce, T., Scholes, B., Steinbrecher, R., Tallamraju, R., Taylor, J., and Zimmerman, P.: A global model of natural volatile organic compound emissions, Journal of Geophysical Research: Atmospheres, 100, 8873-8892, https://doi.org/10.1029/94JD02950, 1995.

Haagen-Smit, A. J.: Chemistry and Physiology of Los Angeles Smog, Industrial & Engineering Chemistry, 44, 1342-1346, 10.1021/ie50510a045, 1952.

Han, J., Liu, Z., Hu, B., Zhu, W., Tang, G., Liu, Q., Ji, D., and Wang, Y.: Observations and explicit modeling of summer and autumn ozone formation in urban Beijing: Identification of key precursor species and sources, Atmospheric Environment, 309, 119932, https://doi.org/10.1016/j.atmosenv.2023.119932, 2023.

Ji, X., Hu, Q., Wang, X., Deng, B., Sun, Z., Wang, Z., Hong, Q., Tang, S., Zhang, W., Xing, C., Zhang, C., and Liu, C.: Variations in Vertical Distributions of O_3, Its Precursors, and Formation Sensitivity in Beijing, China, Based on Ground-Based Remote Sensing, Environmental Science & Technology, 59, 13333-13342, 10.1021/acs.est.5c04527, 2025.

Killus, J. P. and Whitten, G. Z.: Background reactivity in smog chambers, Int. J. Chem. Kinet., 22, 547-575, https://doi.org/10.1002/kin.550220602, 1990.

Lefohn, A. S., Malley, C. S., Smith, L., Wells, B., Hazucha, M., Simon, H., Naik, V., Mills, G., Schultz, M. G., Paoletti, E., De Marco, A., Xu, X., Zhang, L., Wang, T., Neufeld, H. S., Musselman, R. C., Tarasick, D., Brauer, M., Feng, Z., Tang, H., Kobayashi, K., Sicard, P., Solberg, S., and Gerosa, G.: Tropospheric ozone assessment report: Global ozone metrics for climate change, human health, and crop/ecosystem research, Elementa: Science of the Anthropocene, 6, 10.1525/elementa.279, 2018.

Li, G., Lei, W., Zavala, M., Volkamer, R., Dusanter, S., Stevens, P., and Molina, L. T.: Impacts of HONO sources on the photochemistry in Mexico City during the MCMA-2006/MILAGO Campaign, Atmos. Chem. Phys., 10, 6551-6567, 10.5194/acp-10-6551-2010, 2010.

Li, Q., Zhang, L., Wang, T., Wang, Z., Fu, X., and Zhang, Q.: "New" Reactive Nitrogen Chemistry Reshapes the Relationship of Ozone to Its Precursors, Environmental Science & Technology, 52, 2810-2818, 10.1021/acs.est.7b05771, 2018.

Li, Q., Su, G., Li, C., Liu, P., Zhao, X., Zhang, C., Sun, X., Mu, Y., Wu, M., Wang, Q., and Sun, B.: An investigation into the role of VOCs in SOA and ozone production in Beijing, China, Science of The Total Environment, 720, 137536, https://doi.org/10.1016/j.scitotenv.2020.137536, 2020.

Liu, T., Hong, Y., Li, M., Xu, L., Chen, J., Bian, Y., Yang, C., Dan, Y., Zhang, Y., Xue, L., Zhao, M., Huang, Z., and Wang, H.: Atmospheric oxidation capacity and ozone pollution mechanism in a coastal city of southeastern China: analysis of a typical photochemical episode by an observation-based model, Atmos. Chem. Phys., 22, 2173-2190, 10.5194/acp-22-2173-2022, 2022.

Liu, Y., Lu, K., Li, X., Dong, H., Tan, Z., Wang, H., Zou, Q., Wu, Y., Zeng, L., Hu, M., Min, K.-E., Kecorius, S., Wiedensohler, A., and Zhang, Y.: A comprehensive model test of the HONO sources constrained to field measurements at rural North China Plain, Environ Sci Technol, 53, 3517-3525, 10.1021/acs.est.8b06367, 2019.

Lurmann, F. W. and Carter, W. P. L.: Evaluation of a detailed gas-phase atmospheric reaction mechanism using environmental chamber data, Atmospheric Environment. Part A. General Topics, 25, 2771-2806, https://doi.org/10.1016/0960-1686(91)90206-M, 1991.

Ma, J., Xue, M., Tang, G., Tong, S., Hu, B., Zhang, X., Li, X., and Wang, Y.: ROx Budgets and O_3 Formation during Summertime at Xianghe Suburban Site in the North China Plain, Advances in Atmospheric Sciences, 38, 1209-1222, 10.1007/s00376-021-0327-4, 2021.

Metzger, A., Dommen, J., Gaeggeler, K., Duplissy, J., Prevot, A. S. H., Kleffmann, J., Elshorbany, Y., Wisthaler, A., and Baltensperger, U.: Evaluation of 1,3,5 trimethylbenzene degradation in the detailed tropospheric chemistry mechanism, MCMv3.1, using environmental chamber data, Atmos. Chem. Phys., 8, 6453-6468, 10.5194/acp-8-6453-2008, 2008.

https://doi.org/10.5194/egusphere-2025-3956
Preprint. Discussion started: 12 September 2025
© Author(s) 2025. CC BY 4.0 License.

Nelson, B. S., Liu, Z., Squires, F. A., Shaw, M., Hopkins, J. R., Hamilton, J. F., Rickard, A. R., Lewis, A. C., Shi, Z., and Lee, J. D.: The effect of different climate and air quality policies in China on in situ ozone production in Beijing, Atmos. Chem. Phys., 24, 9031-9044, 10.5194/acp-24-9031-2024, 2024.

Pinho, P. G., Pio, C. A., and Jenkin, M. E.: Evaluation of isoprene degradation in the detailed tropospheric chemical mechanism, MCM v3, using environmental chamber data, Atmospheric Environment, 39, 1303-1322, https://doi.org/10.1016/j.atmosenv.2004.11.014, 2005.

Pierce, J. A., Carter, W. P. L., Luo, D., and Malkina, I. L.: Environmental chamber study of maximum incremental reactivities of volatile organic compounds, Atmospheric Environment, 29, 2499-2511, https://doi.org/10.1016/1352-2310(95)00149-S, 1995b.

Pusede, S. E., Steiner, A. L., and Cohen, R. C.: Temperature and Recent Trends in the Chemistry of Continental Surface Ozone, Chemical Reviews, 115, 3898-3918, 10.1021/cr5006815, 2015.

Qin, Z., Liu, Y., Bai, W., Zhang, G., Xu, B., Liu, Y., Geng, C., Zhang, N., Zhao, X., and Yang, W.: Integrating the updated HONO formation mechanism to better understand urban O_3 formation chemistry, Environmental Pollution, 368, 125674, https://doi.org/10.1016/j.envpol.2025.125674, 2025.

Qu, H., Wang, Y., Zhang, R., Liu, X., Huey, L. G., Sjostedt, S., Zeng, L., Lu, K., Wu, Y., Shao, M., Hu, M., Tan, Z., Fuchs, H., Broch, S., Wahner, A., Zhu, T., and Zhang, Y.: Chemical Production of Oxygenated Volatile Organic Compounds Strongly Enhances Boundary-Layer Oxidation Chemistry and Ozone Production, Environmental Science & Technology, 55, 13718-13727, 10.1021/acs.est.1c04489, 2021.

Shek, K. Y., Zeren, Y., Guo, H., Li, M., Liu, M., Huang, B., and Lyu, X.: Insights on In-Situ Photochemistry Associated with Ozone Reduction in Guangzhou during the COVID-19 Lockdown, Atmosphere, 13, 212, https://www.mdpi.com/2073-4433/13/2/212, 2022.

Slater, E. J., Whalley, L. K., Woodward-Massey, R., Ye, C., Lee, J. D., Squires, F., Hopkins, J. R., Dunmore, R. E., Shaw, M., Hamilton, J. F., Lewis, A. C., Mehra, A., Worrall, S. D., Bacak, A., Bannan, T. J., Coe, H., Percival, C. J., Ouyang, B., Jones, R. L., Crilley, L. R., Kramer, L. J., Bloss, W. J., Vu, T., Kotthaus, S., Grimmond, S., Sun, Y., Xu, W., Yue, S., Ren, L., Acton, W. J. F., Hewitt, C. N., Wang, X., Fu, P., and Heard, D. E.: Evaluating the sensitivity of radical chemistry and ozone formation to ambient VOCs and NO_x in Beijing, Atmos. Chem. Phys., 21, 2125-2147, 10.5194/acp-21-2125-2021, 2021.

Tan, Z., Lu, K., Dong, H., Hu, M., Li, X., Liu, Y., Lu, S., Shao, M., Su, R., Wang, H., Wu, Y., Wahner, A., and Zhang, Y.: Explicit diagnosis of the local ozone production rate and the ozone-NO_x-VOC sensitivities, Science Bulletin, 63, 1067-1076, https://doi.org/10.1016/j.scib.2018.07.001, 2018.

Wang, X., Liu, T., Bernard, F., Ding, X., Wen, S., Zhang, Y., Zhang, Z., He, Q., Lü, S., Chen, J., Saunders, S., and Yu, J.: Design and characterization of a smog chamber for studying gas-phase chemical mechanisms and aerosol formation, Atmos. Meas. Tech., 7, 301-313, 10.5194/amt-7-301-2014, 2014.

Wang, Y., Guo, H., Zou, S., Lyu, X., Ling, Z., Cheng, H., and Zeren, Y.: Surface O_3 photochemistry over the South China Sea: Application of a near-explicit chemical mechanism box model, Environmental Pollution, 234, 155-166, https://doi.org/10.1016/j.envpol.2017.11.001, 2018.

Wang, Y., Gao, W., Wang, S., Song, T., Gong, Z., Ji, D., Wang, L., Liu, Z., Tang, G., Huo, Y., Tian, S., Li, J., Li, M., Yang, Y., Chu, B., Petäjä, T., Kerminen, V. M., He, H., Hao, J., Kulmala, M., Wang, Y., and Zhang, Y.: Contrasting trends of PM(2.5) and surface-ozone concentrations in China from 2013 to 2017, Natl Sci Rev, 7, 1331-1339, 10.1093/nsr/nwaa032, 2020.

Wang, Y., Yao, N., Liu, Y., Li, S., Ma, P., Liao, Z., Ren, X., Li, S., Chu, B., Ma, Q., Xin, J., Ma, Y., Quan, J., and He, H.: Campaign for Direct In Situ Study of Residual Layer Chemistry in Urban Beijing, Bulletin of the American Meteorological Society, 106, E625-E641, https://doi.org/10.1175/BAMS-D-24-0127.1, 2025.

Wyche, K. P., Rickard, A. R., Metzger, A., Monks, P. S., Ellis, A. M., Dommen, J., Baltensperger, U., Jenkin, M. E., and Pilling, M. J.: Gas phase precursors to anthropogenic secondary organic aerosol: Using the Master Chemical Mechanism to probe detailed observations of 1,3,5-trimethylbenzene photo-oxidation, Atmospheric Environment, 44, 5423-5433, https://doi.org/10.1016/j.atmosenv.2009.09.043, 2010.

Xuan, H., Zhao, Y., Ma, Q., Chen, T., Liu, J., Wang, Y., Liu, C., Wang, Y., Liu, Y., Mu, Y., and He, H.: Formation mechanisms and atmospheric implications of summertime nitrous acid (HONO) during clean, ozone pollution and double high-level PM2.5

https://doi.org/10.5194/egusphere-2025-3956
Preprint. Discussion started: 12 September 2025
© Author(s) 2025. CC BY 4.0 License.

and O_3 pollution periods in Beijing, Science of The Total Environment, 857, 159538, https://doi.org/10.1016/j.scitotenv.2022.159538, 2023.

Xuan, H., Liu, J., Zhao, Y., Cao, Q., Chen, T., Wang, Y., Liu, Z., Sun, X., Li, H., Zhang, P., Chu, B., Ma, Q., and He, H.: Relative humidity driven nocturnal HONO formation mechanism in autumn haze events of Beijing, npj Climate and Atmospheric Science, 7, 193, 10.1038/s41612-024-00745-8, 2024.

Zhang, J., An, J., Qu, Y., Liu, X., and Chen, Y.: Impacts of potential HONO sources on the concentrations of oxidants and secondary organic aerosols in the Beijing-Tianjin-Hebei region of China, Science of The Total Environment, 647, 836-852, https://doi.org/10.1016/j.scitotenv.2018.08.030, 2019.

Zheng, H., Gen, M., Sun, Y., Xu, W., Ma, N., Su, H., Cheng, Y., Wang, S., Xing, J., Zhang, S., Xue, L., Xue, C., Mu, Y., Tian, X., Matsuki, A., and Song, S.: Rapid hydrolysis of NO_2 at High Ionic Strengths of Deliquesced Aerosol Particles, Environmental Science & Technology, 58, 7904-7915, 10.1021/acs.est.3c08810, 2024.